

Strong evidence for the influence of solar cycles on a Late Miocene lake system revealed by biotic and abiotic proxies

A.K. Kern ^{a,*}, M. Harzhauser ^a, W.E. Piller ^b, O. Mandic ^a, A. Soliman ^{b,c}

^a Natural History Museum Vienna, Geological-Paleontological Department, Burgring 7, 1010 Vienna, Austria

^b Institute of Earth Sciences, Graz University, Heinrichstrasse 26, 8010 Graz, Austria

^c Tanta University, Faculty of Sciences, Geology Department, Tanta 31527, Egypt

ARTICLE INFO

Article history:

Received 26 September 2011

Received in revised form 8 February 2012

Accepted 12 February 2012

Available online 22 February 2012

Keywords:

Miocene

Solar cycles

Lake Pannon

Magnetic susceptibility

Natural gamma radiation

Ostracoda

ABSTRACT

The Late Miocene paleogeography of central Europe and its climatic history are well studied with a resolution of c. 10⁶ years. Small-scale climatic variations are yet unresolved. Observing past climatic change of short periods, however, would encourage the understanding of the modern climatic system. Therefore, past climate archives require a resolution on a decadal to millennial scale.

To detect such a short-term evolution, a continuous 6-m-core of the Paleo-Lake Pannon was analyzed in 1-cm-sample distance to provide information as precise and regular as possible. Measurements of the natural gamma radiation and magnetic susceptibility combined with the total abundance of ostracod shells were used as proxies to estimate millennial- to centennial scale environmental changes during the mid-Tortonian warm period.

Patterns emerged, but no indisputable age model can be provided for the core, due to the lack of paleomagnetic reversals and the lack of minerals suitable for absolute dating. Therefore, herein we propose another method to determine a hypothetical time frame for these deposits.

Based on statistical processes, including Lomb–Scargle and REDFIT periodograms along with Wavelet spectra, several distinct cyclicities could be detected. Calculations considering established off-shore sedimentation rates of the Tortonian Vienna Basin revealed patterns resembling Holocene solar-cycle-records well. The comparison of filtered data of Miocene and Holocene records displays highly similar patterns and comparable modulations. A best-fit adjustment of sedimentation rate results in signals which fit to the lower and upper Gleissberg cycle, the de Vries cycle, the unnamed 500-year- and 1000-year-cycles, as well as the Hallstatt cycle. Each of these cycles has a distinct and unique expression in the investigated environmental proxies, reflecting a complex forcing-system. Hence, a single-proxy-analysis, as often performed on Holocene records, should be considered cautiously as it might fail to capture the full range of solar cycles.

© 2012 Elsevier B.V. All rights reserved.

1. Introduction

Understanding climate-driving mechanisms is a crucial topic in many current research projects from various scientific fields due to the high impact on all life on Earth. Studying recent climate systems is essential to recognize modern climatic patterns; though, future predictions require insights into past climatic evolution.

Unfortunately, historic reports of climatic parameters are scarce. Western scientists started recording temperature and precipitation since 1850 (Versteegh, 2005). This time span, however, covers mainly that part of history where climate was already highly influenced by humans (Tiwari and Ramesh, 2007). Furthermore, direct

measurements of sun's emitted energy dates back only to the first satellite documentation from the year 1978 (e.g. Versteegh, 2005; Tiwari and Ramesh, 2007; Lockwood, 2009; Gray et al., 2010). Thus, both observations are too short to allow unequivocal conclusions on natural climate behavior. Despite this problematic issue, the combination of direct measurements of solar energy by satellites as well as weather stations around the globe, verified the positive correlation of sun and climate (Beer et al., 2000; Versteegh, 2005). Temperature and precipitation patterns are influenced by energy sent off by the sun, reaching the Earth's atmosphere as so-called cosmic rays. Though the first impression, this pattern is inconstant. Regular changes could be linked to the sun's movement (Charcátová, 2000; Versteegh, 2005) and phenomena such as solar eruptions or the quasi-periodic in- and decrease of sunspots.

Sunspots, appearing as dark spots on the sun's surface, were recorded already by ancient Chinese astronomers (Hoyt and Schatten, 1998). More intensive studies were possible due to the invention of first telescopes culminating finally in the direct

* Corresponding author. Tel.: +43 1 52177 250; fax: +43 1 52177 459.

E-mail addresses: andrea.kern@nhm-wien.ac.at (A.K. Kern),

mathias.harzhauser@nhm-wien.ac.at (M. Harzhauser), werner.piller@uni-graz.at

(W.E. Piller), oleg.mandic@nhm-wien.ac.at (O. Mandic), ali.soliman@uni-graz.at

(A. Soliman).

observation and measurements by satellites (Eddy, 1976; Hoyt and Schatten, 1998). An iterative process in respect to the amount of visible sunspots was observed for the first time by Schwabe (1844), who reported a steady in- and decrease within a 11-year cyclicity (= Schwabe cycle or sunspot-cycle). Although sunspots cause a local decrease in emitted energy, the surrounding surface of the sun releases energy in a higher degree. Accordingly, a higher number of sunspots leads to more solar power hitting the Earth's atmosphere. Satellite measurements revealed these variations to account for 0.1% of the oscillation of solar irradiance within 11 years (Lean et al., 1995). Longer cycles may modulate the intensity of the shorter ones, causing extreme climatic events. Phases of almost completely lacking sunspots are discussed to correlate with the cool historical periods, such as the Spörer Minimum (1460–1550), the Dalton Minimum (1790–1830) and the Maunder Minimum (1645–1715) (Eddy, 1976; Lean et al., 1995; Versteegh, 2005 and therein). Thus, the longest phase of dearth on sunspots during the late 17th century, also called the Maunder Minimum or the Little Ice Age, is discussed to be severely influenced by solar forcing (Eddy, 1976; Robock, 1979; Mörner, 2010).

The Gleissberg cycle is one of the slightly longer solar cycles, probably modulating the Schwabe cycle (Wolf, 1862; Gleissberg, 1939). Firstly assumed to have a duration of 88-years, Ogurtsov et al. (2002) detected a characteristic split into a low-frequency band signal of 50–80 years and a high-frequency signal between 90 and 140 years.

Except for the Gleissberg cycle, direct satellite measurements display neither enough data nor time to proof the existence of other cycles. Therefore, proxy data are necessary to postulate and test such longer periodicities. The best established method is the analysis of time series of atmospheric radioactive isotopes such as ^{14}C (e.g. Stuiver and Braziunas, 1989; Damon and Sonett, 1991; Perislykh and Damon, 2003; Solanki et al., 2004) and ^{10}Be (Beer et al., 1990; Wagner et al., 2001; Usoskin et al., 2003; Solanki et al., 2004) in combination with the total solar irradiance (TSI; e.g. Bard et al., 2000). Their production-rate in the atmosphere is directly linked to the amount of incoming cosmic rays, and thus allows a direct reconstruction of solar intensity (Tiwari and Ramesh, 2007).

Consequently, a ~208 year-cyclicity, named de Vries or Suess cycle (Damon and Sonett, 1991; Stuiver and Braziunas, 1993; Wagner et al., 2001), is documented in various Holocene records (e.g. Schimmelmann et al., 2003; Raspopov et al., 2008; Taricco et al., 2009; Incarbona et al., 2010; Di Rita, 2011). It might as well be present from historical sunspot observations (Ma and Vaquero, 2009). Its influence on several climatic parameters has been discussed by Raspopov et al. (2007), who document a non-linear response of the climate system in various geographic regions.

Longer time-period sun cycles display frequencies of ~500 to 550 years (Stuiver et al., 1995; Chapman and Shackleton, 2000), ~1000 years (Stuiver et al., 1995; Chapman and Shackleton, 2000; Debret et al., 2007) and ~2400 years (Hallstatt cycle) (Damon and Sonett, 1991; Chrcátová, 2000; Nederbragt and Thurow, 2005). Although these cycles appear in many studies their impact on climate is poorly resolved. A climate-link to wind stress and humidity/aridity is suggested only for the Hallstatt cycle (Nederbragt and Thurow, 2005). No direct nexus is published for the other cycles, but highly expected since they all depend on solar activity.

Most studies on solar cycles are confined to Pleistocene and Holocene records due to limits set by the radioactive isotopes (Bard and Frank, 2006). A further problem is the availability of solid age-models with an appropriate high time-resolution. Therefore, studies outside the ^{14}C -range usually concentrate on annually preserved records such as lake varves (Milana and Lopez, 1998; Raspopov et al., 2008; Lenz et al., 2010).

Nearly all the studies, however, center on a single proxy, which may represent only individual feedback patterns to solar activity.

Therefore, we try to achieve a more detailed and complex picture by analyzing three independent but coeval 600-data-point-sets comprising natural gamma radiation, magnetic susceptibility and the total amount of ostracods. The target is a 6-m-long core with Upper Miocene lake sediments of ancient Lake Pannon in the Vienna Basin (Austria).

2. Geological setting

Lake Pannon (Fig. 1) covered the Pannonian Basin complex in central and south-eastern Europe during the Miocene and Pliocene. It formed at c. 11.6 Ma when the marine Paratethys Sea retreated to the east. The remaining lake was a brackish and slightly alkaline lacustrine system (Magyar et al., 1999; Harzhauser et al., 2004; Piller et al., 2007; Harzhauser and Mandic, 2008). Lake Pannon experienced its maximum extension of c. 290,000 km² during the Tortonian between 10.5 and 10.0 Ma.

In the Vienna Basin, this phase is recorded by the Bzenec Formation, which crops out at the opencast pit Hennersdorf (Fig. 1), situated app. 10 km south of the center of Vienna. It currently exposes roughly 14 m of blue-grey clays and silts with several mollusc coquinas and scattered plant debris. Information about the lithology and biostratigraphy of the Hennersdorf section was already published in more detail by Harzhauser and Mandic (2004) and Harzhauser et al. (2008). The mollusc fauna represents assemblages of the regional middle Pannonian stage, corresponding to the middle Tortonian (Magyar et al., 1999). Magnetostratigraphy allowed a correlation with the long normal chron C5n (Magyar et al., 1999). Correlation with astronomically tuned well-logs in the Vienna Basin suggests an absolute age of 10.5–10.4 Ma for the section (Harzhauser et al., 2004; Lirer et al., 2009).

In 2009, a 15-m-long core was drilled in the clay pit of which the lower 6 m could be drilled without core break. The core comprises grey-green silty clay with occasionally occurring plant debris and mollusc coquinas; bioturbation is rare. The lower 6 m are rather homogenous; a slight fining upward trend occurs in the lower part indicated by a gradual shift from clayey silt (samples 1540 to 1230) to silty clay (sample 1231 to 979). Upsection follows again silty clay (sample 980 to 940). The upper part of the core, which is not analyzed herein, displays a coarsening upward trend with increasing amounts of silt and few fine sand layers in the uppermost part (Fig. 2a).

3. Methods

3.1. Sampling

The herein analyzed 6-m-core with a diameter of 15 cm was drilled at the clay pit of Hennersdorf (N48°05'52.6" E016°21'15.8"). We focus on the samples from core-depth 1540 cm (named sample 1540) up to 941. This results in a total of 600 continuous and equal-spaced data points. All parts of the core were marked with a 1-cm-scale on the outside, before they were divided into two halves. One of these is kept for future studies in the Natural History Museum Vienna.

First, lithology and macroscopic fossil content such as mollusc debris and plant fossils were evaluated for each sample-cm. By the same strict sample distance, 600 measurements were taken for natural gamma radiation and magnetic susceptibility. Natural gamma radiation was measured with a hand held "Compact Gamma Surveyor" (Scintillation Gamma Radiometer) and the magnetic susceptibility was measured with an "SM-20" magnetic susceptibility meter with a sensitivity of 10⁻⁶ SI units (GF Instruments, Brno, Czech Republic). Afterwards the core was cut into 1-cm-thick slices for micropaleontological investigation. Each of these samples was dried, weighed and further treated with H₂O₂ and sieved with 125, 250 and 500 μm

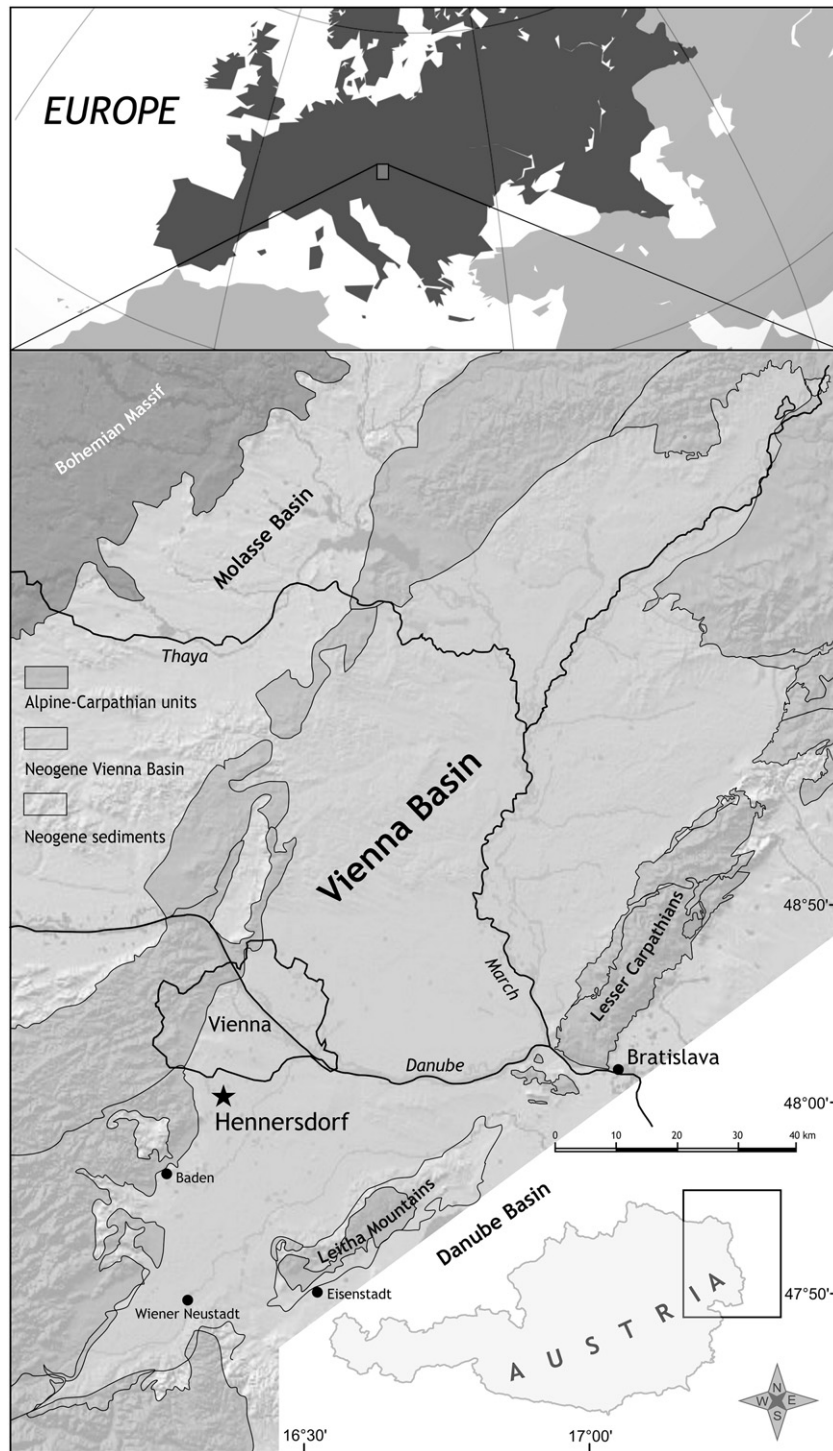


Fig. 1. Geological map of the Vienna Basin showing the position of the investigated core at Hannersdorf inside the Vienna Basin (modified after Harzhauser et al., 2004).

mesh-size sieves. The total number of ostracod valves was evaluated for all 600 samples (articulated specimens were counted as 1). These data were then standardized for a sample weight of 100 gram (Table 1). The mollusc debris was counted at a range scale from 0 to 3 (0 = no shells; 1 = rare debris or single shells; 2 = loose coquina; 3 = dense coquina) (Fig. 2b).

3.2. Data analysis

Each of the 600 data was first transferred into percentages, before an arcsin-root-transformation was applied to ensure a higher

comparability within the different proxy data for further statistical processing (Linder and Berchtold, 1976; Zuschin and Hohenegger, 1998). The software PAST (Hammer et al., 2001) was used to remove trends in all data curves and to produce a 3-point-smoothing for clearer presentation (Fig. 2c, d, e).

PAST was used to perform spectral analysis including REDFIT (Schulz and Mudelsee, 2002) and wavelet analysis. REDFIT is a Fortran 90 program, which allows overcoming the common problem in paleontology of unevenly spaced time series by fitting a first-order autoregressive process. Though sample distance is strictly consistent, due to lithologically unnoticeable changes in sedimentation rate

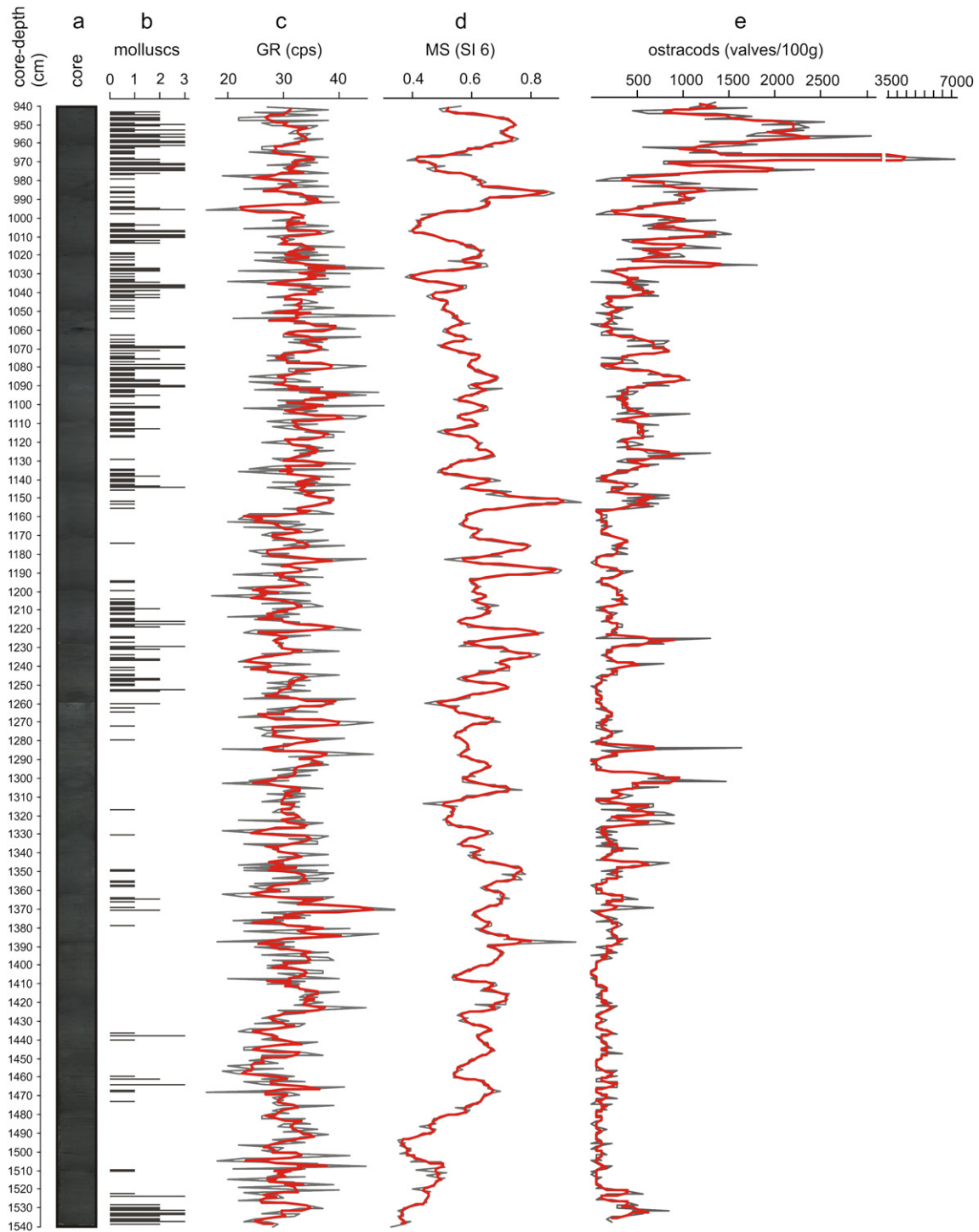


Fig. 2. Illustration of the raw data (600 data points for each proxy; core depth in cm corresponds to sample numbers 1540 to 940). The core picture (a) shows the rather homogeneous sedimentology; mollusc abundance (b) is indicated on a semi-quantitative scale (0 = no shells; 1 = rare debris or single shells; 2 = loose coquina; 3 = dense shell bed); note that the coquinas are autochthonous (Harzhauser and Mandic, 2004). Natural gamma radiation (GR) is given in cps (c), magnetic susceptibility (MS) in Si-units (d) and the total abundance of ostracods is calculated for 100 g sediment (e). Grey lines are raw data, red lines represent the 3-point running mean.

small imbalances within the sample distances might occur. Monte-Carlo method is applied to test a bias-corrected spectrum. The frequency values of the Lomb–Scargle and REDFIT periodograms were then transferred into depth-domain to indicate the statistically relevant cycles in centimeters. Additionally, wavelet analysis was performed to detect potential non-stationary periodicities. The same methods were applied to the ^{14}C based Holocene record of solar

activity of Solanki et al. (2004). Periodicities indicated by the Lomb–Scargle and REDFIT periodograms were used as target for a Gaussian bandpass filter with the AnalySeries program (Paillard et al., 1996). This is a frequency-selective filtering procedure, which removes unwanted frequency components from the time series. The bandpass filtering was applied to all three data-sets and is state-of-the-art in modern cyclostratigraphy (Weedon, 2003).

4. Results

4.1. Natural Gamma Radiation (GR)

The GR-record fluctuates between 16 and 52 cps over the whole investigated core-section and displays a high frequency oscillation (Fig. 2c). The record may be divided into three parts, although variations along the section appear not as significant as between certain samples. The first one reaches from sample 1540 to 1370 and comprises a rapid succession of serrated, often sharply cut, peaks. Around sample 1370 a strong peak in values occurs, marking the onset of an interval with a moderately serrated motif of comparatively low values without trend. This second part is terminated around sample 1052 with another strong positive peak. Above follow gradually decreasing values with several strongly negative peaks arranged between comparatively higher values (Fig. 2c). To gain more insight into this record, a spectral analysis was performed on the 3-point-running-mean data set (Fig. 3a). This displays three strong frequencies which pass the 95% confidence interval. The most prominent cycles have wavelengths of 116.9 and 37.7 cm (Fig. 3a). An additional bundle of peaks in the spectral analysis suggests very prominent cycles between 8.8 and 15.2 cm (Fig. 3a), supporting the intuitive interpretation. Comparable cycles are indicated by the REDFIT analysis, which points to cycles with periodicities of 6.4, 8.8 and 12.8 cm,

passing the 99% confidence interval (Fig. 3b). These results are supported by the wavelet analysis, which visualizes an especially intense signal with periodicities of 6.4–8.8 cm and around 12.6–15.4 cm (Fig. 4g). The two longer periodicities at 116.9 and 37.7 cm are very distinct as well in the wavelet analysis.

Filtering these data to the long periodicity, centered at 116.9 cm, shows constant amplitudes throughout the section except for a slight decline in the uppermost part (Fig. 4e). Applying a Gaussian filter centered at 37.7 cm, shows low but constantly increasing amplitudes in the lower part (Fig. 4f). The middle part displays high amplitudes and an excellent fit with the raw data. In the upper core interval the signal becomes weaker again. This pattern fits well to the wavelet analysis which suggests the strongest expression of this cycle in the middle core interval. A filter at 15.2 cm (from 12.7 to 19.0 cm) reveals the best fit with the raw data with the highest amplitudes between samples 1400 and 1330 (Fig. 4d). The signal intensity is weakening afterwards but displays phases of increasing amplitudes at core intervals 1290–1220, 1170–1145, 1105–1075 and 1000–950 at the top. Further, data centered at 8.8 cm (from 7.5 to 10.7 cm) reveal a similar shape in the lower and upper half of the section, with two strong and weak phases being topped by a dominating one (Fig. 4c). The shortest of all filtered curves centered at 6.4 cm (from 5.7 to 7.3 cm) is constantly in- and decreasing without phases of strong manifestation (Fig. 4b). Again, these phases correlate to strong signals in the wavelet analysis.

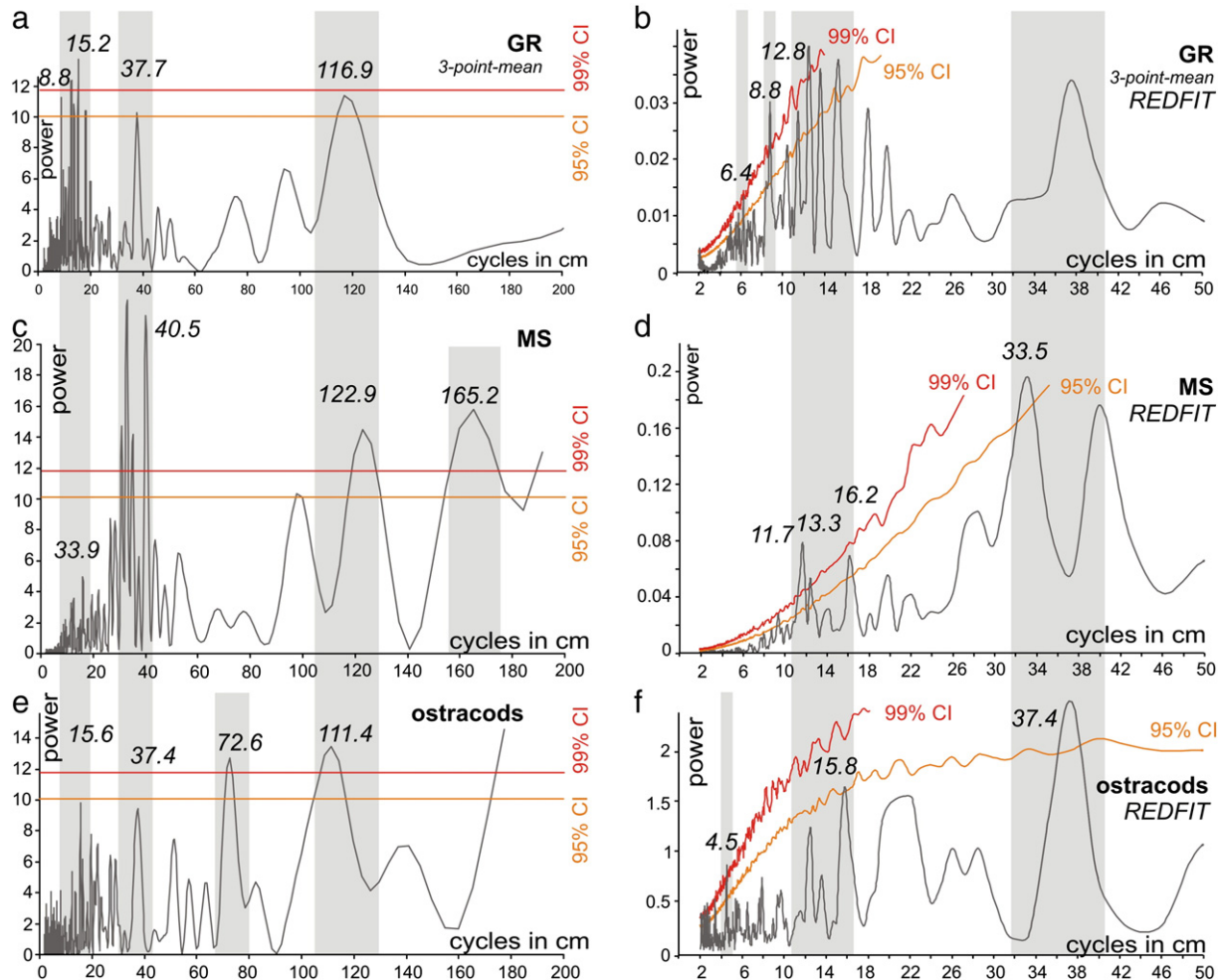


Fig. 3. Lomb–Scargle (left; a, c, e) and REDFIT (right; b, d, f) periodograms display repetitive periodicities in each of the three proxy-data-sets. Longer frequencies are better revealed in the power spectra, whilst short cyclicities are better supported in the REDFIT-analysis. Frequencies of 37.4 to 40.5 cm, 111.4 to 122.9 cm are evident in all proxies, while others appear only in one or two.

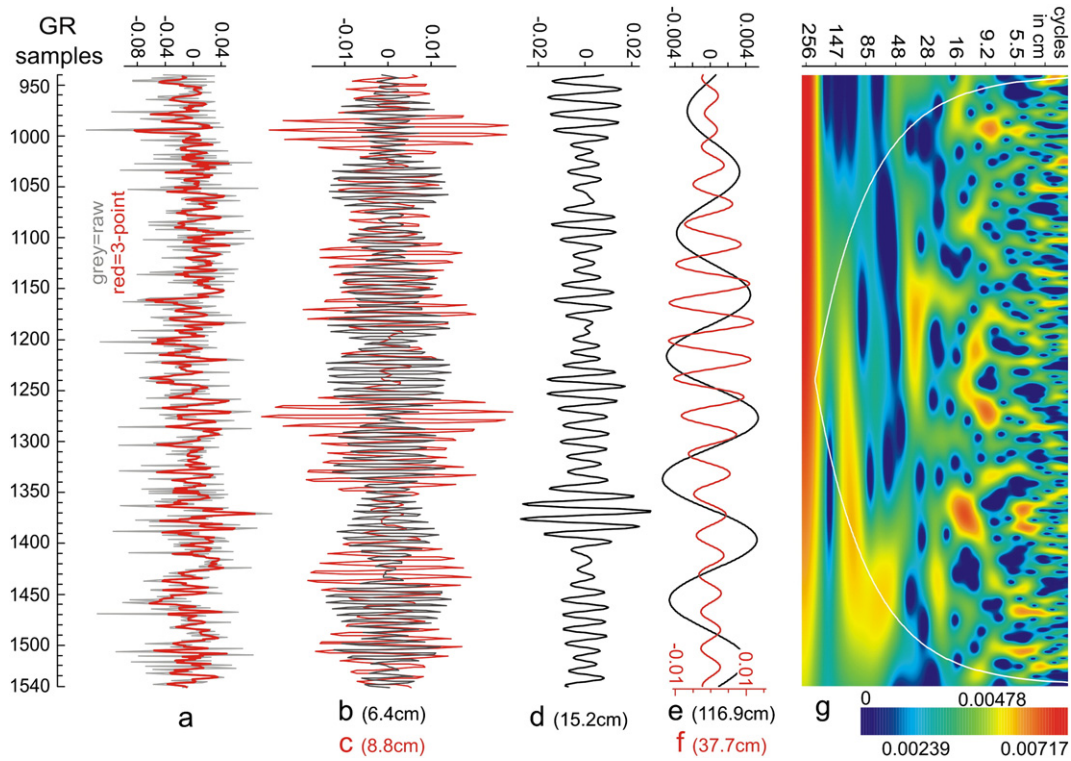


Fig. 4. Natural gamma radiation: a: original data (root/arcsin-transformed and detrended) were filtered according to the dominant periods revealed by the periodograms in Fig. 3. Gaussian filter were applied centering at b: 6.4 cm (range from 5.7 to 7.3 cm), c: 8.8 cm (7.5–10.7 cm), d: 15.2 cm (12.7–19.0 cm), e: 37.7 cm (32.9–44.1 cm) and f: 116.9 cm (104.8–132.2 cm); g: wavelet analyses clearly show the presence of these periodicities including the high frequency signals and also document the high-frequency modulation of the various signals.

4.2. Magnetic susceptibility (MS)

The MS record (Fig. 2d) is strongly fluctuating with values ranging from 0.3 to 0.9 SI units. The raw data and the 3-point-running-mean graph already suggest a fairly regular pattern between high and low MS values. High-frequency oscillations, as in the GR record, are missing. The record shows a serrated motif with overall increasing values up to sample 1388. Above follows a serrated interval up to sample 1152 without significant trend. The upper core interval is characterized by overall decreasing values, which are arranged in rapidly fluctuating values up to sample 1030 and a decreasing frequency above.

The serration is also expressed in a very significant signal in the spectral analysis, indicating a strong periodicity at 33.9 cm and at 40.5 cm (Fig. 3c). This interval is also evident in the autocorrelation of the data. A third peak, passing the 95% confidence interval, occurs at 122.9 cm next to a fourth at 165.2 cm. The REDFIT analysis supports the peak at 33.5 cm and suggests two further high-frequency cycles at 11.7–13.3 cm, passing the 99% confidence interval, and a second weaker one at 16.2 cm (Fig. 3d). These cycles are clearly visible in the wavelet analysis (Fig. 5f), which documents their presence in the interval 1260–1130 cm. The wavelet illustrates clearly the lack of shorter cycles, which differs from the other two proxies.

Filtering the data according to the peaks in the Lomb–Scargle periodograms shows a continuously decreasing signal at 165.2 cm (152.6–180.1 cm) (Fig. 5e) and a steady signal at 122.9 cm (109.6–139.9 cm) (Fig. 5d). The Gaussian filter at 36.6 cm reveals strongest signals in the lower part of the core up to sample 1450 and in the top between samples 1050 and 950 (Fig. 5c). The high frequency filter centered at 15.6 cm documents highest amplitudes in the middle between samples 1270 and 1180 (Fig. 5b).

4.3. Ostracods

The samples yield mainly rich ostracod assemblages of usually disarticulated specimens. The total abundance is fluctuating drastically, ranging from only 3 shells up to 7247 per 100 gram sediment, but usually stays distinctly below 1000 specimens (Fig. 2e).

Except for a first small peak with about 500 to 800 valves up to sample 1524, the lower part of the core shows very low abundances up to sample 1407. A slow increase in ostracods persists upwards to sample 1278 with two peaks of up to 1600 valves. Moderate values of 200–300 valves characterize the following interval up to sample 1160 being interrupted by two single peaks with more than 700 specimens. Above, abundances are oscillating at higher levels around few hundred specimens up to peaks with 1300 specimens. At sample 1030 low values occurs again, before the numbers of shells are significantly increasing but still strongly fluctuating. The highest abundances occur in the top part of the core including several samples with extraordinary high numbers (977 to 951 cm) (Fig. 2e).

The Lomb–Scargle periodogram reveals only two significant signals with periodicities of 72.6 and 111.4 cm (Fig. 3e). Small-scale frequencies are indicated by peaks at 15.6 and 37.4 cm, but do not reach the 95% confidence interval. Both peaks, however, are much more significant in the REDFIT spectrum which verifies cycles with periodicities of 15.8 and 37.4 cm (Fig. 3f). This method suggests the presence of an even shorter cycle with a periodicity of 4.5 cm, passing even the 99% interval-boundary.

These high-frequency cycles are also indicated in the wavelet analysis (Fig. 6g), which documents their presence especially in the intervals 1540–1270 and 1080–940 while they are insignificant in the interval between. The long 111.4-cm-signal is very noticeable and continuous (Fig. 6g). In contrast, the 37.4-cm-signal is most prominent in the lower half of the core and the 15.8-cm-signal is best expressed in the middle of the record (Fig. 6g).

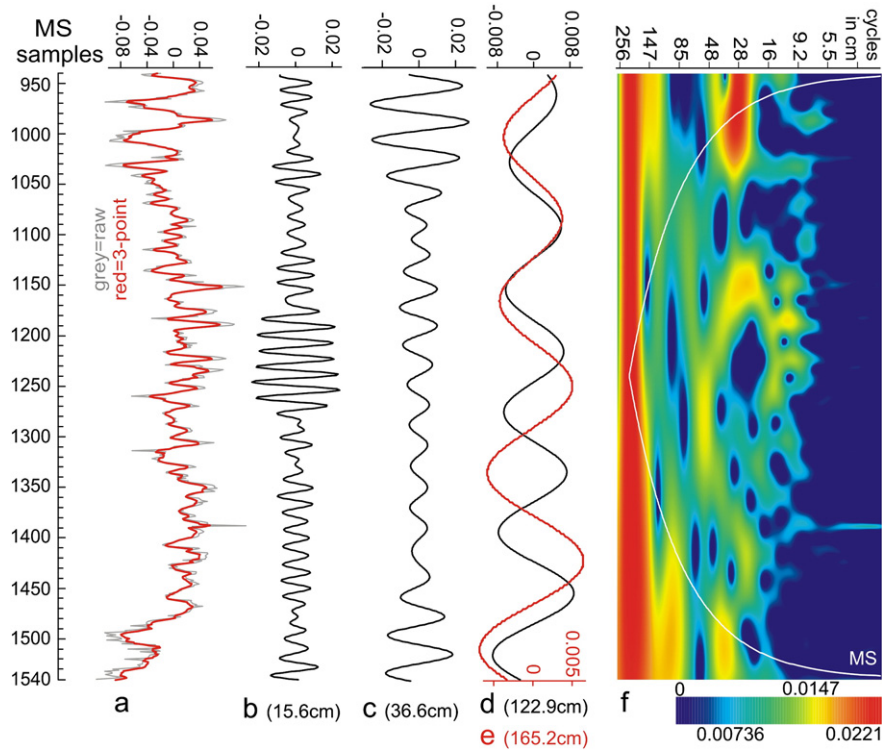


Fig. 5. Magnetic susceptibility: a: original data (root/arcsin-transformed and detrended) were filtered according to the dominant periods revealed by the periodograms in Fig. 3. Gaussian filter were applied centering at b: 15.6 cm (range from 13.0 to 19.6 cm), c: 36.6 cm (32.1–42.6 cm), d: 122.9 cm (109.6–139.9 cm) and e: 165.2 cm (152.6–180.1 cm); f: the wavelet analyses clearly show the presence of the low frequency periodicities. High frequency signals around 15.6 cm are strongest in the middle part of the core, whilst higher frequency signals as seen in the gamma radiation data are completely missing.

Filtering these data centered at 111.4 cm, documents the continuous expression of that long-period cycle throughout the section with a slight increase towards the top (Fig. 6f). A comparable pattern with a more intense increase of intensity is visible in the filtered data centered at 72.6 cm (Fig. 6d). The filtered 37.4-cm-cycle increases in amplitude and is very prominent in the lower half of the core, but becomes weakly expressed in the upper part of the core from sample 1150 onwards (Fig. 6e). Also the shortest of the filtered cycles centered at 15.6 cm is strongly variable (Fig. 6c). Starting with a weak signal up to approximately sample 1440, the amplitude increases significantly up to sample 1290. Afterwards it becomes very weakly expressed and rises again in the upper part of the core from sample 1070 onwards. The small-scale signal centered at 8.8 cm (7.5–10.7 cm) displays a very strong influence in the lower part of the core (Fig. 6b), followed by a rapid decrease and a mainly weak significance up to sample 1040, where another peak occurs. No significant strong phase follows further upwards.

4.4. Similarities and dissimilarities in the proxy records

All three proxies reveal different patterns and rhythms. Only two of the cycles are present in all records: the most prominent one has a periodicity of c. 116 cm and the second one centers around 37 cm (Fig. 3a, c, e). Moreover, all three records are characterized by a series of high-frequency cycles ranging between 8.8 and 16 cm. Unique periodicities are the strong 165-cm-cycle in the MS record (Fig. 3c) and the 72.6 cm cycle in the ostracod record (Fig. 3e). The filtered data, too, suggest that the three proxies responded differently to the various cycles. Hence, the maximum amplitudes in the ~37-cm-cycle appear in the MS record (Fig. 5c) during phases of a weak expression of that cycle in the other proxies (Figs. 4f, 6d). These display maxima during weaker phases of the MS record. Similar relations occur in the filtered high-frequency records of the ~15.6-cm-cycle (Figs. 4d,

5b, 6c). Additionally, the GR and ostracod data reveal a small-scale signal around 8.8 cm, documenting a higher degree of small-scale forcing (4c, 6b).

5. Discussion

The reason for the described differences in the patterns may probably be proxy-inherent. The total amount of ostracods is suggested to reflect favorable lake-bottom conditions. An earlier study on the ostracods from the Hennersdorf section (Fig. 1) has documented severe oxygenation crises leading to reduced numbers of ostracods (Harzhauser et al., 2008). According to that paper, the assemblages are dominated by five taxa (*Cyprideis*, *Hemicytheria*, *Lineocypris/Caspionella*, *Amplocypris*, *Loxochoncha*) which occur in rather constant ratios despite the strongly fluctuating numbers of individuals. The rapid decline of ostracod abundance is therefore explained by unfavorable conditions due to poor bottom water oxygenation. Further, lowered nutrient supply might also be responsible for low counts.

The GR signal, in contrast, is not solely depending on lake-bottom conditions. Generally, it is interpreted as an expression of the presence of detectable radioactive isotopes emitted by Potassium-, Uranium- and Thorium-bearing minerals (Blum et al., 1997), which are mainly transported into the lake by rivers or wind. Similarly, the MS signal is mainly a function of detrital input of carrier minerals such as magnetite and pyrrhotite (Stockhausen and Thouveny, 1999; Ellwood et al., 2000). A clear correlation between high MS values and increased precipitation in Holocene lake sediments in India was explained by Warriar and Shankar (2009) through an increased input of pedogenic magnetic particles and by intensification of chemical weathering. A relation between high water levels, humid climate and high MS signatures was also documented for Lake Hunlun in Mongolia (Hu et al., 1999) and Lake Chalco in Mexico (Lozano-García and Ortega-Guerrero, 1994). Contrary to this, Lake

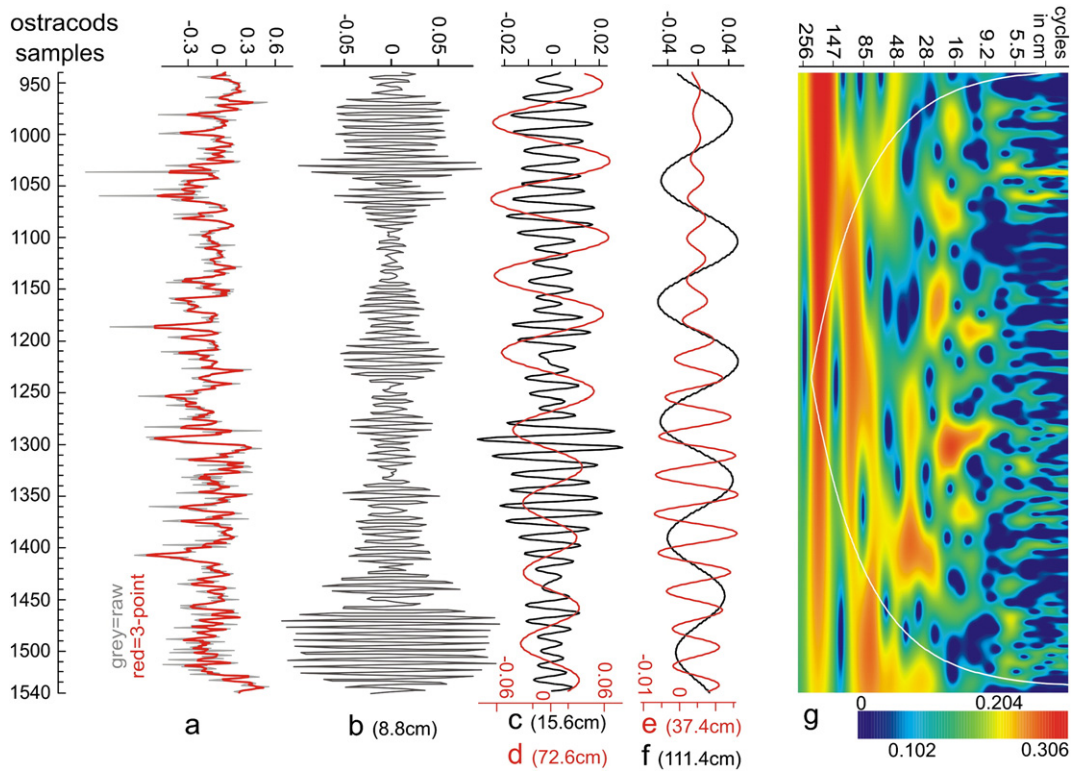


Fig. 6. Total abundance of ostracods per 100 g sediment: a: original data (root/arc-sin-transformed and detrended) were filtered according to the dominant periods revealed by the periodograms in Fig. 3. Gaussian filter were applied centering at b: 8.8 cm (range from 7.5 to 10.7 cm), c: 15.6 cm (13.0–19.6 cm), d: 72.6 cm (63.4–85.0 cm), e: 37.4 cm (32.7–53.7 cm) and f: 111.4 cm (100.3–125.2 cm); g: these periodicities are also evident in the wavelet analyses showing the strong modulation of the 15.6 cm and 34.4 cm periodicities.

Mosoko in Tanzania displays lowest MS values during lake level highs and wet conditions, when heavy minerals are stored in the littoral area (Garcin et al., 2006). This seemingly simple relation between transport and MS signal, however, is strongly challenged by the formation of authigenic ferromagnetic sedimentary greigite. This iron-sulfide is frequently found in Miocene sediments of Lake Pannon and related water bodies (Babinszki et al., 2007; Vasiliev et al., 2010) and formed through a series of microbially mediated reactions (Roberts et al., 2011). Hence, the measured MS-log may reflect a mixture of input of carrier minerals and authigenic modification in the lake sediment.

In addition to these factors, causing different response patterns in the studied proxies, there may be a time lag present as well. The ostracod record is expected to reflect the rise and fall of populations in a very high temporal resolution without recognizable temporal bias. Similarly, the GR record is suggested to reflect more or less coeval changes in environmental conditions. The MS signal, in contrast, may be altered by diagenetic processes and the bacteria induced formation of greigite may have occurred below the sediment/water interface resulting in a time lag. These processes might also be responsible for the absence of the high-frequency cycles in the MS signal, whereas these cycles were unaffected in the total ostracod abundance and GR records.

5.1. From depth to time domain – a hypothesis

There is no possibility to reconstruct an accurate absolute age-model for the herein studied core. Any transformation of the data from depth into time domain remains hypothetical. Yet knowing its stratigraphic position, we are able to link it to sediment accumulation rates in the Vienna Basin. Hence, astronomically tuned middle Tortonian drilled basinal successions of Lake Pannon indicate average sedimentation rates of c. 0.65 mm/yr (= 15.4 yr/cm) (Lirer et al., 2009).

Slightly higher sedimentation rates have to be expected for the core as the drill site was closer to the shore than the above mentioned basinal drillings and within the influence of a delta system in about 4–6 km distance (Harzhauser et al., 2008). As the 6-m-long core is too short to capture the smallest Milankovitch cycles, the highly significant cycles might represent sub-Milankovitch cycles represented by solar cycles most likely.

To test this hypothesis we used the proven sedimentation rate of Lirer et al. (2009) of 0.65 mm/yr for a time domain transformation of the detected cyclicities. Those result in periodicities of ~570 yr for the dominant 37-cm-cycle and ~240 yr for the 15.6-cm-cycle. Other cycles detected (72.6 cm; ~115 cm; 165.2 cm), would represent ~1120, ~1800, and ~2540 years. These values, except for the 1800-yr-cycle, are very close to the periodicities of Holocene solar cycles (e.g. Beer et al., 1990; Stuiver and Braziunas, 1993; Solanki et al., 2004; Yin et al., 2007). Based on this hypothesis we performed a best-fit adjustment of the sedimentation rate. Only a slightly increased sedimentation rate up to 0.73 mm/yr (= 13.7 yr/cm), results in periodicities of 205.5–213.7, 501.4–516.5, 994.6 and 2271 years (taking the average values of 15–15.6, 33.6–37.7, 72.6, 165.2 cm, respectively), which is in full agreement with the several postulated periodicities of Holocene solar cycles (Solanki et al. (2004)). Moreover, a strong cycle appears with a periodicity of roughly 1600 years (1526–1684 years or 111.4–122.9 cm). This cycle cannot be attributed to any known solar cycle but agrees well with the poorly understood ~1500-cycle (Bond et al., 2001). Recently, this cycle was interpreted as a feedback mechanism to internal oceanic processes or the modulation of other solar cycles (Bard and Frank, 2006; Debret et al., 2007). Debret et al. (2009) further discussed changing intensity of the Atlantic circulation as trigger mechanism. Thus, up to now the origin of this cycle remains enigmatic but no indication for a solar origin of the 1500-year-cycle could be documented (Debret et al., 2007, 2009). Nevertheless, in Holocene records it is

well documented from marine records and from far distant continental areas, such as Canada (Campbell et al., 2000) and Arabia (Parker et al., 2006). Weber et al. (2010) discovered a ~1500-yr-cycle even in Upper Miocene lake deposits of northern Greece. This suggests that this cycle is not strictly linked to the Pleistocene-Holocene glacial climate system.

5.2. Holocene solar cycles

Applying the best-fit sedimentation rate of 0.73 mm/yr to the time domain transformation of the core, results in a total of 8220 years of Miocene time reflected in the core. This allows a comparison with Holocene records, where many studies already detected the existence of solar cycles and discussed their influence on Earth's climate. The longest continuous record of solar activity based on radioactive isotopes documents almost 12,000 years of solar activity (Solanki et al., 2004). This huge data set is based on a comparison between ^{10}Be and ^{14}C from tree rings and is available at <http://www.ncdc.noaa.gov/paleo/recons.html>. Periods and quasi-periods of solar activity were previously detected in these data also by Yin et al. (2007), who also performed a wavelet analysis.

To achieve a better understanding of these solar patterns, we utilized the Solanki-et-al.-data as well and processed them with the same methods as our Miocene records. Besides creating a power spectrum and wavelet analysis similar to Yin et al. (2007), we applied the REDFIT method and filtered the data according to the dominant periodicities to visualize the shifts in amplitude of the various solar cycles through time (Figs. 7 and 8).

Our analysis is in good agreement with the results of Yin et al. (2007). Both approaches indicate the de Vries cycle with periodicities of 225-years and an unnamed 352-yr-cycle (Fig. 7a and b). In addition to the peak at 225 years, our analysis shows an additional peak at 208 years suggesting slight shifts in the duration of the individual

de Vries cycles (Fig. 7a). Peaks at 443 (441 in Yin et al., 2007), 522 and 561 years are also analogous to Yin et al. (2007). All these signals might represent a single quasi-periodic 500-year-cyclicity (Fig. 7a). Although this cycle is constantly expressed in the record (Fig. 8g), the splitting of its signal points to some variation of its frequency (Fig. 8g). The next significant peak occurs at 970 years, indicating the unnamed 1000-yr-cycle. Finally, the Lomb–Scargle periodogram shows a strong peak at 2210 to 2227 years, which represents the Hallstatt cycle (Fig. 7a). The Gleissberg cycle does not appear in the spectral analysis but is expressed by two very significant peaks above the 99% confidence interval at 88 and 151 years in the REDFIT analysis (Fig. 7b). This is explained by the presence of too much noise in the huge data set, which is removed using the REDFIT spectrum (Schulz and Mudelsee, 2002). This solar cycle displays a wide frequency band and temporal variation in power with a lower Gleissberg band of 50–80 years and an upper Gleissberg band of 90–140 years fitting excellently to the two-fold signal in the REDFIT spectrum (Ogurtsov et al., 2002; Ma, 2009). The REDFIT analysis documents also the presence of a very prominent quasi-210-yr-periodicity of the de Vries cycle (Fig. 7b). Considering the wavelet spectrum, it is obvious, that the very high-frequency solar cycles (less than 60 years of duration) are poorly resolved (Fig. 8i), corresponding to the wavelet analysis of Yin et al. (2007). This may most likely be caused by the presence of noise due to the irregularities in these solar cyclicities. The lower Gleissberg cycle, however, is still visible with its highest intensity from 5500 to 12,000 years (Fig. 8i). The upper Gleissberg cycle is also expressed with a prominent phase between 2500 and 8000 years.

An important fact is the absence of any 1500-year-cycle (Fig. 7). This is a strong proof, that this periodicity is no solar cycle as suggested by Bond et al. (2001) but might result from other feed-back mechanisms (e.g. Braun et al., 2005; Versteegh, 2005; Bard and Frank, 2006; Xapsos and Burke, 2009).

The filtered data demonstrate a considerable modulation of the different solar cycles (Fig. 8c to h). The 1000-year-cycle shows a constant decrease in amplitude during the Holocene (Fig. 8h). The filtered quasi-500-yr-component has a comparable trend (Fig. 8g); its amplitude decreased strongly resulting in a moderate minimum around 5000–3500 B.C., then increased slightly again and becomes insignificant during the last 1000 years. In contrast, the expression of the 2210-yr Hallstatt cycle increases throughout the Holocene (Fig. 8f). The filtered 209-yr-component, representing the de Vries cycle, shows a much more complex pattern (Fig. 8e). It strongly alternates between high and low amplitude phases, but is overall steadily strengthening. Two major break-downs occurred around 5700–4500 B.C. and 2200–1500 B.C. The lower and upper Gleissberg cycles are also highly oscillating and display no phase-relation (Fig. 8c). The 151-yr-component develops a phase of extraordinary high amplitudes from about 4000–2500 B.C. and a second weaker phase from 700 B.C. to 200 A.D. (Fig. 8d), roughly coinciding with maxima in the de Vries cycle. The 88-yr-component, in contrast, tends to develop maxima in phases of low amplitude of the de Vries cyclicity.

5.3. Solar cycles in Miocene and Holocene times – a comparison

The close resemblance of the Lomb–Scargle periodograms of the Miocene records and the Holocene ones (Fig. 9) is strongly supporting our interpretation of the detected cycles as expression of variations in solar activity. The appearance of the 1500-yr-cycle as an “Earth-system-immanent cycle” is the major difference between both diagrams. This observation is of substantial importance as this cycle is also known from a Late Miocene lake in Greece (Weber et al., 2010) as well as it was indicated previously for Lake Pannon (Paulissen and Luthi, 2011).

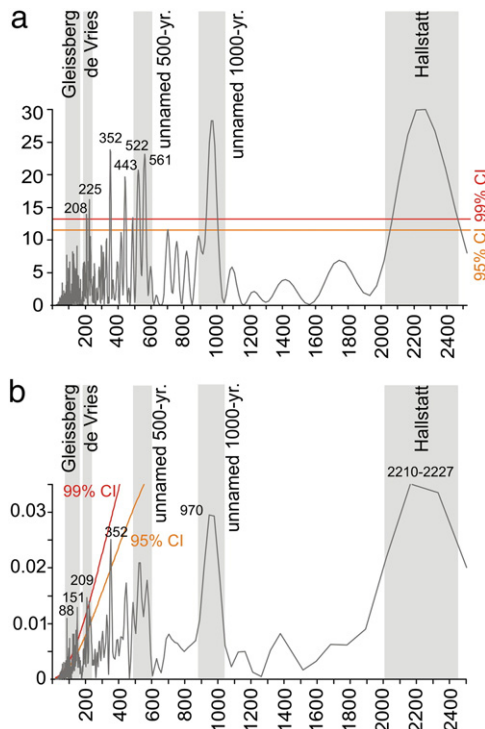


Fig. 7. Lomb–Scargle (a) and REDFIT (b) periodograms performed on the Holocene sunspot numbers from Solanki et al. (2004). The results of the power spectrum is comparable to results of Yin et al. (2007) and detects all known solar cycles from the de Vries cycle onwards. The REDFIT analysis, however, is able to detect also the lower and upper Gleissberg cycles. Similarly to the Miocene record, the sample resolution excludes an expression of the 11-years-Schwabe cycle.

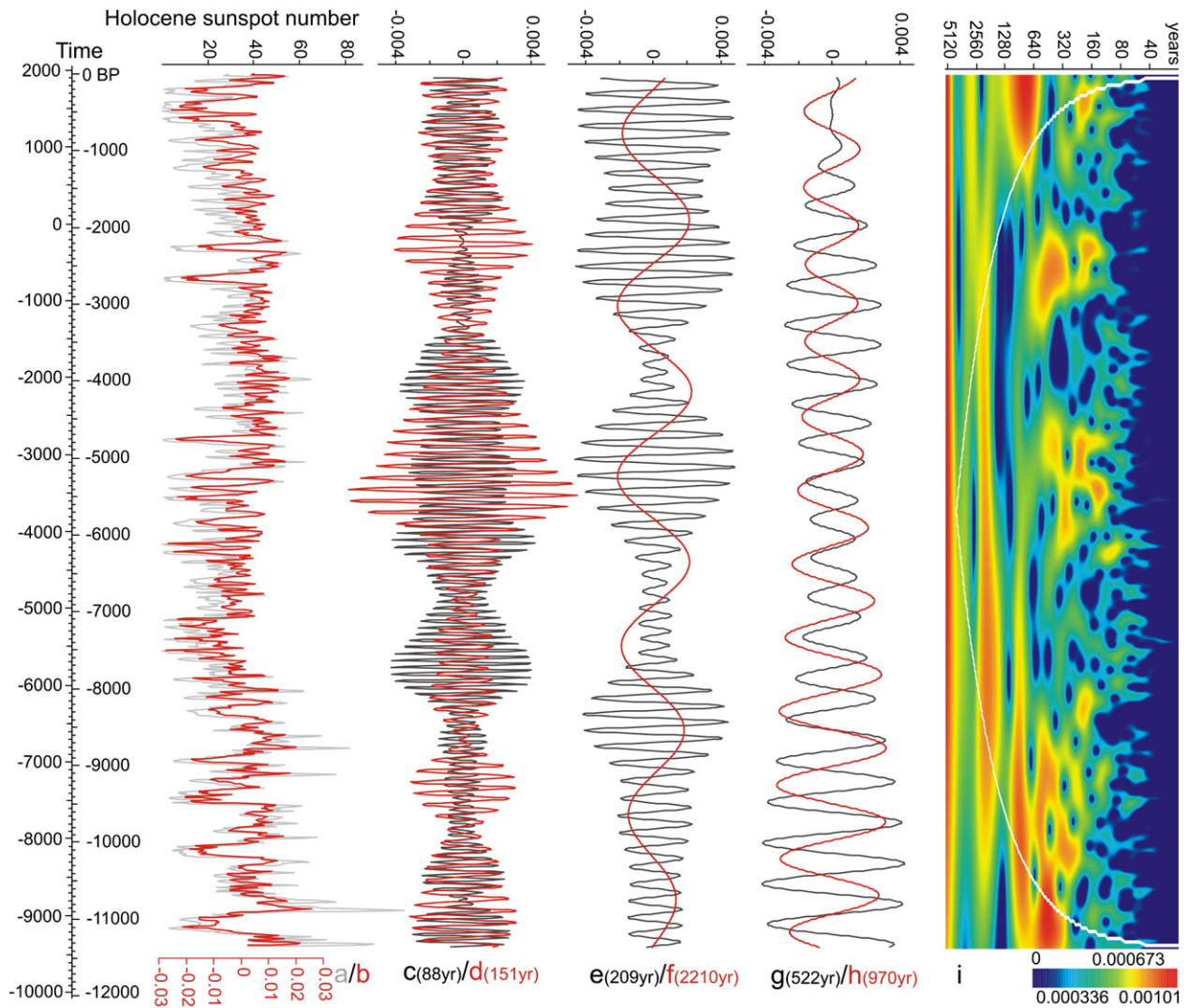


Fig. 8. Holocene solar activity (Solanki et al., 2004): a: calculated sunspot numbers and b: the root/arc-sin-transformed and detrended data. Gaussian filters have been applied to the data according to the dominant periods revealed by the periodograms in Fig. 7. These filters are centered at c: 88 years (range from 79 to 98 yrs), d: 151 years (135.2–171.0 yrs), e: 209 years (192.2–229.0 yrs), f: 2210 years (1976.3–2512.6 yrs), g: 522 years (480.1–571.8 yrs) and at h: 970 years (874.1–1089.3 yrs). The strong modulation of the signals is also evident in the wavelet analysis (i).

As shown by the filtered Holocene solar activity data (Fig. 8a), the various cycles are strongly modulated through time. Especially the de Vries cycle appears as succession of high and low amplitude phases. The wavelet analyses show an unsteady expression of the centennial-scaled solar cycles. A strikingly similar pattern arises from the filtered MS data of Lake Pannon. The time transformed data reveal comparable durations of high-amplitude and low-amplitude phases and a near identical modulation of the signal. This coincidence in patterns may be taken as further support for our hypothesis, that the proxies may reflect the imprint of solar cycles.

Our results suggest that the response of certain proxies to certain solar cycles may be significantly different. High amplitudes of certain solar-cycles in the isotope-based data of Solanki et al. (2004) will not necessarily appear with the same pattern in other proxy records. This may complicate the creation of a “master-target-curve” for the Holocene and even more for the Miocene. Therefore, the possibility of a non-uniform response of different environmental proxies within the same geographic area to a common external trigger should be considered in analysis of Holocene data as well.

5.4. Ecological interpretation

The ecological impact of solar forcing is still enigmatic. Solar energy dispersion varies globally, thus, its influence on climate has to be studied on a regional scale. Climate observations around the earth are able to detect a solar effect, but are increasingly obliterated by anthropogenic interference (Gray et al., 2010). Versteegh (2005) discussed a link between the position of the Intertropical Convergence Zone (ITCZ) and solar activity, but concluded that global data are needed to test this hypothesis.

Especially, sea- and lake-levels are sensitive to variations in solar activity (Yousef, 2006; Bruckman and Ramos, 2009). Cosmic rays influence climatic patterns due to their influence on cloud formation (Friis-Christensen and Svensmark, 1997). The total cloud cover is an often neglected but important factor for local climate since it is in correlation with the Earth’s surface temperature as well as snow/rainfall. These in turn, determine how much water is introduced into the lake-system and how much is removed due to evaporation (Friis-Christensen and Svensmark, 1997; Gray et al., 2010). Because of their smaller water body, lakes are more sensitive to small climatic changes. Several lakes seem to reflect even the shortest known solar

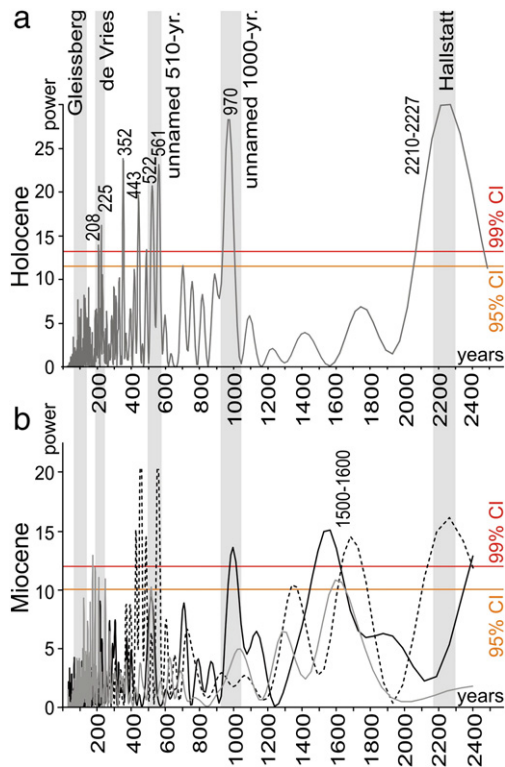


Fig. 9. A comparison of the Lomb–Scargle periodogram of the Holocene sunspot activity with time-converted periodograms of the Miocene proxy data. The overall similarity of the patterns is striking. Moreover, the appearance of the non-solar ~1500-yr-cycle in the Miocene data sets is obvious. GR: gray line, MS: dashed line, ostracodes: black line.

cycle, the 11-year Schwabe cycle (Yousef, 2006). The impact of the solar cycles on the various lakes, however, is not uniform and each lake system has to be considered separately. Similarly, the impact of the de Vries cycle depends on geographic region. This solar cycle may be expressed, e.g., by exceptional flooding events or by phases of increased aridity, pointing to a very complex sun-climate-feedback-mechanism with strong regional character (Raspovov et al., 2008). Nevertheless, significant solar-cycle-related changes in lake ecology and lake level have been variously documented for Holocene records (Vos et al., 1997; Yousef, 2006; Di Rita, 2011). Therefore, an influence of solar forcing on the environments surrounding the Miocene Lake Pannon and its hydrology is equally presumable.

The statistic analyses of the three different proxy data clearly document repetitive shifts with periodicities of c. 10–15, 37–40, 72.6, 110–120 and 165 cm (Fig. 3). Based on our age-model the dominant of these cycles have periods of c. 209, 510, 995, 1600 and 2300 years (Fig. 7b). The intensity and modulation of these various cycles for each of the proxies is individually varying. This is explained by the fact that all three proxies are linked to different environmental factors. The GR record suggests small scaled, high-frequency oscillations of the lake level which are mainly forced by the de Vries cycle. Additionally, an impression by the upper and lower Gleissberg cycles is indicated by the REDFIT analysis (Fig. 3b). The overall GR pattern indicates a slight transgressive tendency up to sample 1370, a rather stable phase thereafter, terminated by another transgressive pulse around sample 1052. Afterwards the decreasing values suggest a slight shallowing. This interpretation is well supported by the increasing amount of silt and the increasing amount of shell hash and coquinas. The transgressive phases, in contrast, are reflected by low settlement by molluscs (Fig. 2b).

The ostracod record follows this overall deepening trend but differ significantly in details. This indicates that a much more complex ecological response, instead of a simple lake-level fluctuation, is reflected

by the bottom-dwelling ostracods. The de Vries cycle explains only small parts of their record; in contrast, a decadal scaled cycle close to the lower Gleissberg signal and a 500-yr-cycle dominate in the REDFIT analysis. Especially the strong dominance of the Gleissberg cycle, which coincides with the weak expression of other cycles, between the base and sample 1450, is reflected by regular small-scale variations of the lake-bottom conditions.

The 500-yr-cycle is also the dominant factor in the MS signal, pointing to a causal relation between MS signal and lake-bottom-water oxygenation. It is strongly expressed in the lower and the top part of the core and has a moderately strong signal in the middle part. Phases which reflect a significant impact of the de Vries cycle coincide with a low expression or decrease of other cyclicities. Information on higher frequencies appears to have been lost due to post-sedimentary processes such as bacteria-induced greigite formation.

All three Miocene (GR, MS, ostracods) and the Holocene records document that a low expression of the various solar cycles is reflected by low fluctuations in the environmental proxies suggesting comparatively stable – though not necessarily favorable – conditions (Fig. 10). Moreover, we document that the various solar cycles are reflected not uniformly by different paleoenvironments and proxies. Finally, the modulation of the cycles in the filtered data is fully comparable with that of Holocene records suggesting that the Miocene system of Lake Pannon was influenced by identical variations of solar radiation.

6. Conclusions

The investigated continuous 6-m-core of Tortonian lake sediments clearly displays regular fluctuations and modulations within three different environmental proxies (natural gamma radiation, magnetic susceptibility, total abundance of ostracods). Lomb–Scargle and REDFIT periodograms next to wavelet spectra of all data sets reveal distinct frequencies. Only few of these are deciphered in all proxy data sets at the same power, while some occur only in two or one proxies.

Converting these frequencies into a time-domain based on previously published sedimentation rates for Lake Pannon in the Vienna Basin, resulted in cyclicities, which agree well with known solar cycles deduced from Holocene sunspot records (Fig. 10). Accepting this as a hypothesis of the observed cycles represent solar cycles, a best-fit adjustment of the sedimentation rate revealed a full fit to the proposed solar cycles. This in turn might be a method to estimate hypothetical sedimentation rates in sedimentary sections for which no age control can be established.

Hence, the Late Miocene lake system seems to reflect the influences of c. 80, 120, 208, 500, 1000, 1500 and 2300 year cyclicities, corresponding to the lower and upper Gleissberg, the de Vries/Suess, the unnamed 500-year, 1000-year and the Hallstatt cycles (Fig. 10). After filtering the data according to the dominant frequencies, the cycles turn out to be strongly modulated, comprising phases of high amplitudes alternating with phases of low amplitudes. To test the solar-forcing-hypothesis, the data are compared with those from the Holocene isotope data of Solanki et al. (2004). The filtered Miocene data correspond strikingly with those of the Holocene records, but a significant difference is the presence of a 350-cycle in the Holocene and the appearance of a 1500-year-periodicity in all three fossil records. The latter one seems to be independent from solar-forcing and represents an “Earth-system-immanent-cycle”.

All proxies reflect the influence of the de Vries, the 500-year-cycle and the above mentioned 1500-year-cycle. Of these, the 500-year-cycle seems to have played a dominant role in the lake system.

The magnetic susceptibility shows further the impact of the long Hallstatt cycle, but tends to resolve short-term variations, such as the Gleissberg cycle (Fig. 10). This problem could be associated to the bacterial activity in the bottom-sediments of Lake Pannon leading

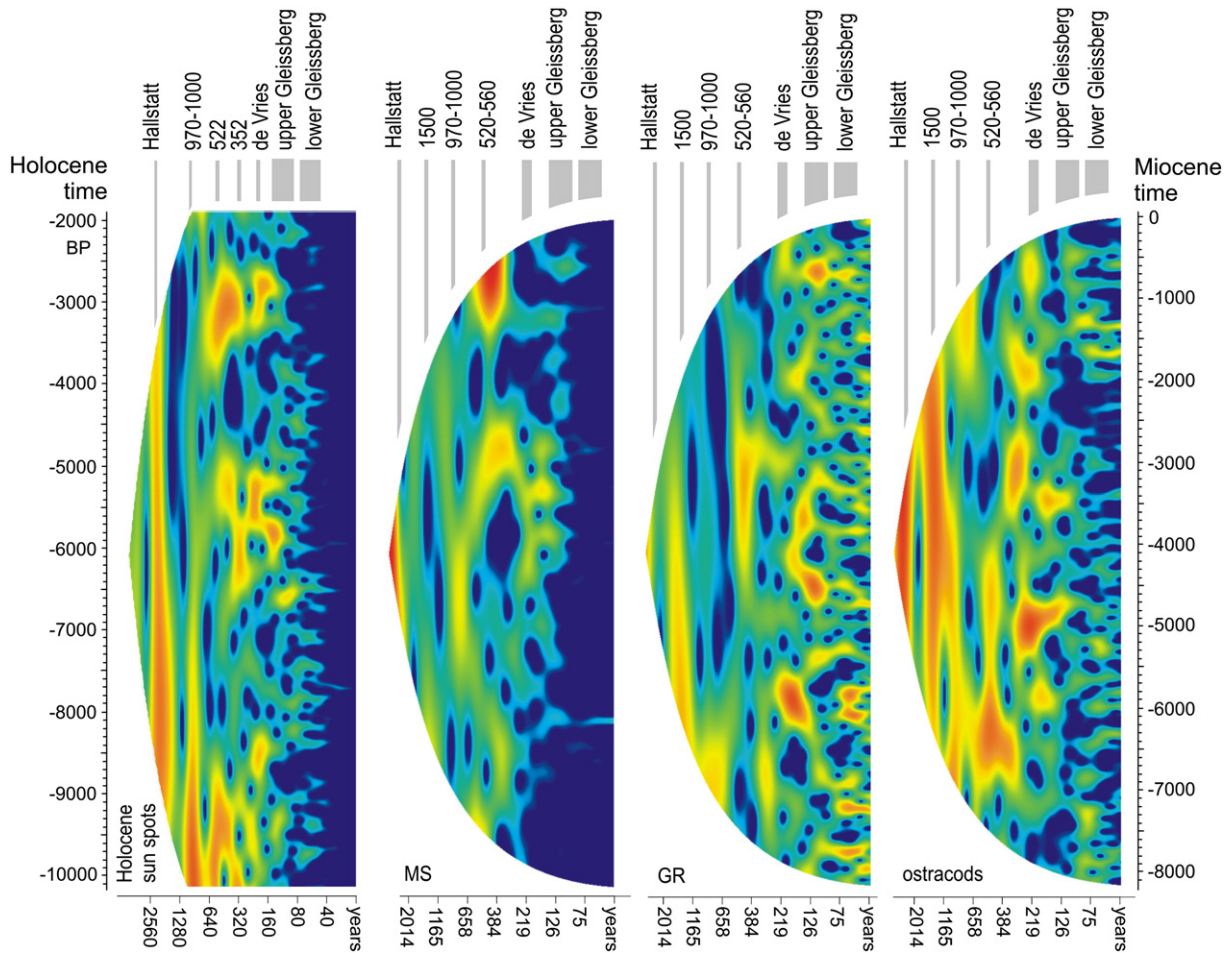


Fig. 10. Comparison of time-transformed wavelet spectra of the Miocene records with an equivalent time span of the Holocene sunspot record from Solanki et al. (2004). The shorter cycles are more intensely revealed in the gamma radiation and ostracod data. Each solar cycle is marked: Lower Gleissberg (50–80 yrs), Upper Gleissberg (90–140 yrs), de Vries/Suess (~208 yrs), ~500-yr cycle and ~1000-yr cycle, Hallstatt (~2300 yrs). In addition a 352-year cycle appears in the Holocene record and a 1500-year cycle in the Miocene data.

to the formation of greigite, which consequently destroyed any original high-frequency signal. The two short Gleissberg cycles are present only in the gamma radiation and ostracod records. Beyond that, it is impossible to detect shorter cycles such as the Schwabe cycle, as one sample roughly corresponds to one decade of Miocene time.

Thus, each proxy responds in a different intensity to certain cycles. While the MS signal seems to be partly overprinted by bacterial activity, the gamma-record is supposed to document input by wind or fluvial systems. It is the most sensitive proxy and largely unaffected by post-sedimentary processes. Therefore this proxy is able to capture very high-frequency oscillations. In contrast, the establishment of hostile bottom conditions leading to low ostracod abundance may be linked to periodically increased lake stratification. Although the latter two processes might be linked, no clear phase relation is evident in the data aside from the 500-year-cycle.

The integrated analysis of different environmental proxies reflects a very complex process of how solar forcing influences climate and environment. The mechanism behind is still enigmatic and even poorly understood during the Holocene. Consequently, a single-proxy analysis, as frequently done in Holocene records, will probably fail to detect the full range of cycles. Still, these observations document the pervasive and persistent influence of changes in solar activity on Earth's climate and regional climate variability even in non-glacial periods.

Supplementary materials related to this article can be found online at [doi:10.1016/j.palaeo.2012.02.023](https://doi.org/10.1016/j.palaeo.2012.02.023).

Acknowledgements

This study is supported by the FWF grant P21414-B16. Further, we want to thank Anton Englert, Anton Fürst, Franz Topka, Andy Leggat and Lisa Schmidinger for core preparation, sample processing and counting of the ostracods. The reviews by Fabrizio Lirer (Istituto Ambiente Marino Costiero, Naples) and Gonzalo Jiménez-Moreno (Universidad de Granada) helped to improve the quality of the paper.

References

- Babinszki, E., Márton, E., Márton, P., Kiss, L.F., 2007. Widespread occurrence of greigite in the sediments of Lake Pannon: implication for environment and magnetostratigraphy. *Palaeogeography, Palaeoclimatology, Palaeoecology* 252, 626–636.
- Bard, E., Frank, M., 2006. Climate change and solar variability: what's new under the sun? *Earth and Planetary Science Letters* 248, 1–14.
- Bard, E., Raisbeck, G., Yiou, F., Jouzel, J., 2000. Solar irradiance during the last 1200 years based on cosmogenic nuclides. *TELLUS, B* 52 (3), 985–992.
- Beer, J., Mende, W., Stellmacher, R., 2000. The role of the sun in climate forcing. *Quaternary Science Reviews* 19, 403–415.
- Beer, J., Blinov, A., Bonani, G., Finkel, R.C., Hofmann, H.J., Lehmann, B., Oeschger, H., Sigg, A., Schwander, J., Staffelbach, T., Stauffer, Suter, M., Wölfli, W., 1990. Use of ^{10}Be in polar ice to trace the 11-year cycle of solar activity. *Nature* 347, 164–166.
- Blum, P., Rabaute, A., Gaudon, P., Allan, J.F., 1997. 14. Analysis of natural gamma-ray spectra obtained from sediment cores with the shipboard scintillation detector of the Ocean Drilling Program: example from leg 1561. *Proceedings of the Ocean Drilling Program. Scientific Results* 156, 183–195.
- Bond, G., Kormer, B., Beer, J., Muscheler, R., Evans, M.N., Showers, W., Hoffmann, S., Lotti-Band, R., Hadjas, I., Bonani, G., 2001. Persistent solar influence on North Atlantic Climate during the Holocene. *Science* 294, 2130–2136.

- Braun, H., Christl, M., Rahmstorf, S., Ganopolski, A., Mangini, A., Kubatzki, C., Roth, K., Kromer, B., 2005. Possible solar origin of the 1,470 year glacial climate cycle demonstrated in a coupled model. *Nature* 438, 208–211.
- Bruckman, W., Ramos, E., 2009. Evidence for climate variations induced by the 11-year solar and cosmic rays cycles. *Proceedings of the International Astronomical Union* 5, 446–448.
- Campbell, I., Campbell, C., Yu, Z., Vitt, D.H., Apps, M., J., 2000. Millennial-scale rhythms in peatlands in the western interior of Canada and in the global carbon cycle. *Quaternary Research* 54, 155–158.
- Chapman, M.R., Shackleton, N.J., 2000. Evidence of 550-year and 1000-year cyclicities in North Atlantic circulation patterns during the Holocene. *The Holocene* 10, 287–291.
- Charcátová, I., 2000. Can origin of the 2400-year cycle of solar activity be caused by solar inertial motion? *Annales Geophysicae* 18, 399–405.
- Damon, P.E., Sonett, C.P., 1991. Solar and terrestrial components of the atmospheric $C-14$ variation spectrum. In: Sonett, C.P., Giampapa, M.S., Methews, M.S. (Eds.), *The sun in time*. The University of Arizona, Tucson, pp. 360–388.
- Debret, M., Bout-Roumazilles, V., Grousset, F., Desmet, M., McManus, J.F., Massei, N., Sebagn, D., Petit, J.-R., Copard, Y., Trentesaux, A., 2007. The origin of the 1500-year climate cycles in Holocene North-Atlantic records. *Climate of the Past* 3, 569–575.
- Debret, M., Sebagn, D., Crosta, X., Massei, N., Petit, J.-R., Chapron, E., Bout-Roumazilles, V., 2009. Evidence from wavelet analysis for a mid-Holocene transition in global climate forcing. *Quaternary Science Reviews* 28, 2675–2688.
- Di Rita, F., 2011. A possible solar pacemaker for Holocene fluctuations of salt-marsh in southern Italy. *Quaternary International*. doi:10.1016/j.quaint.2011.11.030.
- Eddy, J.A., 1976. The Maunder Minimum. *Science* 192, 1189–1202.
- Ellwood, B.B., Crick, R.E., El Hassani, A., Benoist, S.L., Young, R.H., 2000. Magnetosusceptibility event and cyclostratigraphy method applied to marine rocks: detrital input versus carbonate productivity. *Geology* 28, 1135–1138.
- Friis-Christensen, E., Svensmark, H., 1997. What do we really know about the sun-climate connection? *Advances in Space Research* 20, 913–921.
- Garcin, Y., Williamson, D., Taieb, M., Vincens, A., Mathé, E.E., Majule, A., 2006. Centennial to millennial changes in maar-lake deposition during the last 45,000 years in tropical Southern Africa (Lake Masoko, Tanzania). *Palaeogeography, Palaeoclimatology, Palaeoecology* 239, 334–354.
- GLEISSBERG, 1939. *Observatory* 62, 158.
- Gray, L.J., Beer, J., Geller, M., Haigh, J.D., Lockwood, M., Matthes, K., Cubasch, U., Fleitmann, D., Harrison, G., Hood, L., Luterbacher, J., Meehl, G.A., Shindell, D., van Geel, B., White, W., 2010. Solar influence on climate. *Reviews of Geophysics* 48, RG4001.
- Hammer, Ø., Harper, D.A.T., Ryan, P.D., 2001. PAST: Palaeontological Statistics Software package for education and data analysis. *Palaeontologia Electronica* 4 (1), 9.
- Harzhauser, M., Mandic, O., 2004. The muddy bottom of Lake Pannon-a challenge for dreissenid settlement (Lake Miocene; Bivalva). *Palaeogeography, Palaeoclimatology, Palaeoecology* 204, 331–352.
- Harzhauser, M., Mandic, O., 2008. Neogene lake systems in Central and South-Eastern Europe: faunal diversity, gradients and interrelations. *Palaeogeography, Palaeoclimatology, Palaeoecology* 260, 417–434.
- Harzhauser, M., Daxner-Höck, G., Piller, W.E., 2004. An integrated stratigraphy of the Pannonian (Late Miocene) in the Vienna Basin. *Austrian Journal of Earth Science* 95 (96), 6–19.
- Harzhauser, M., Kern, A., Soliman, A., Minati, K., Piller, W.E., Danielopol, D.L., Züschin, M., 2008. Centennial- to decadal scale environmental shifts in and around Lake Pannon (Vienna Basin) related to a major Lake Miocene lake level rise. *Palaeogeography, Palaeoclimatology, Palaeoecology* 270, 102–115.
- Hoyt, D.V., Schatten, K.H., 1998. Group sunspot numbers: a new solar activity reconstruction. *Solar Physics* 179, 189–219.
- Hu, S., Wang, S., Appel, E., Ji, L., 1999. Environmental mechanism of magnetic susceptibility changes of lacustrine sediments from Lake Hulun, China. *Science in China (Series D)* 43, 534–540.
- Incarbona, A., Ziveri, P., Di Stefano, E., Lirer, F., Mortyn, G., Patti, B., Pelosi, N., Sprovieri, M., Tranchida, G., Valletto, A., Albertazzi, S., Bellucci, L.G., Bonanno, A., Bonomo, S., Censi, P., Ferraro, L., Giuliani, S., Mazzola, S., Sprovieri, R., 2010. The impact of the Little Ice Age on coccolithophores in the Central Mediterranean Sea. *Climate of the Past* 6, 795–805.
- Lean, J., Beer, J., Bradley, R., 1995. Reconstructions of solar irradiance since 1610: implications for climate change. *Geophysical Research Letters* 22, 3195–3198.
- Lenz, O.K., Wilde, V., Riegel, W., Harms, F.-J., 2010. A 600 k.y. record of El Niño-Southern Oscillation (ENSO); evidence for persisting teleconnections during the Middle Eocene greenhouse climate of Central Europe. *Geology* 38, 627–630.
- Linder, A., Berchtold, W., 1976. *Statistische Auswertung von Prozentzahlen*. 1–230. Birkhäuser, Basel.
- Lirer, F., Harzhauser, M., Pelosi, N., Piller, W.E., Schmid, H.P., Sprovieri, M., 2009. Astronomically forced teleconnection between Paratethyan and Mediterranean sediments during the Middle and Late Miocene. *Palaeogeography, Palaeoclimatology, Palaeoecology* 275, 1–13.
- Lockwood, M., 2009. Solar change and climate: an update in the light of the current exceptional solar minimum. *Proceedings of the Royal Society A*. doi:10.1098/rspa.2009.0519.
- Lozano-García, M.D.S., Ortega-Guerrero, B., 1994. Palynological and magnetic susceptibility records of Lake Calco, central Mexico. *Palaeogeography, Palaeoclimatology, Palaeoecology* 109, 177–191.
- Ma, L.H., 2009. Gleissberg cycle of solar activity over the last 7000 years. *New Astronomy* 14, 1–3.
- Ma, L.H., Vaquero, J.M., 2009. Is the Suess cycle present in historical naked-eye observations of sunspots? *New Astronomy* 14, 307–310.
- Magyar, I., Geary, D.H., Müller, P., 1999. Palaeogeographic evolution of the Late Miocene Lake Pannon in Central Europe. *Palaeogeography, Palaeoclimatology, Palaeoecology* 147, 151–167.
- Milana, J.P., Lopez, S., 1998. Solar cycles recorded in Carboniferous glacial marine rhythmites (Western Argentina): relationships between climate and sedimentary environment. *Palaeogeography, Palaeoclimatology, Palaeoecology* 144, 37–63.
- Mörner, N.-A., 2010. Solar Minima. Earth's rotation and Little Ice Ages in the past and in the future. *The North Atlantic-European case*. *Global and Planetary Change* 72, 282–293.
- Nederbragt, A.J., Thurov, J., 2005. Geographic coherence of millennial-scale climate cycles during the Holocene. *Palaeogeography, Palaeoclimatology, Palaeoecology* 211, 313–324.
- Ogurtsov, M.G., Nagovitsyn, Y.A., Kocharov, G.E., Jungner, H., 2002. Long-period cycles of the sun's activity recorded in direct solar data and proxies. *Solar Physics* 211, 371–394.
- Paillard, D., Labeyrie, L., Yiou, P., 1996. Macintosh program performs timeseries analysis. *Transactions of the American Geophysical Union* 77, 379.
- Paulissen, W.E., Luthi, S.M., 2011. High-frequency cyclicity in a Miocene sequence of the Vienna Basin established from high-resolution logs and robust chronostratigraphic tuning. *Palaeogeography, Palaeoclimatology, Palaeoecology* 307, 313–323.
- Parker, A.G., Goudie, A.S., Stokes, S., White, K., Hodson, M.J., Manning, M., Kennet, D., 2006. A record of Holocene climate change from lake geochemical analyses in southeastern Arabia. *Quaternary Research* 66, 465–476.
- Perisylak, A.-N., Damon, P.E., 2003. Persistence of the Gleissberg 88-year cycle over the last 12,000 years: evidence from cosmogenic isotopes. *Journal of Geophysical Research* 108, 1003. doi:10.1029/2002JA009390.
- Raspovov, O.M., Dergachev, V.A., Kuzmin, A.V., Kozyreva, O.V., Ogurtsov, M.G., Kolström, T., Lopatin, E., 2007. Regional tropospheric responses to long-term solar activity variations. *Advances in Space Research* 40, 1167–1172.
- Piller, W.E., Harzhauser, M., Mandic, O., 2007. Miocene Central Paratethys stratigraphy – current status and further directions. *Stratigraphy* 4, 71–88.
- Raspovov, O.M., Dergachev, V.A., Esper, J., Kozyreva, O.V., Frank, D., Ogurtsov, M., Kolström, T., Shao, X., 2008. The influence of the de Vries (200-year) solar cycle on climate variations: results from the Central Asian Mountains and their global link. *Palaeogeography, Palaeoclimatology, Palaeoecology* 259, 6–16.
- Roberts, A.P., Chang, L., Rowan, C.J., Horg, C.-S., Florindo, F., 2011. Magnetic properties of sedimentary greigite (Fe_3S_4): an update. *Review of Geophysics* 49, RG1002.
- Robock, A., 1979. The "Little Ice Age": Northern Hemisphere average observations and model calculations. *Science* 206, 1402–1404.
- Schimmelmann, A., Lange, C.B., Meggers, B.J., 2003. Palaeoclimatic and archaeological evidence for a 200-yr recurrence of floods and droughts linking California, Mesoamerica and South America over the past 2000 years. *The Holocene* 13, 763–778.
- Schulz, M., Mudelsee, M., 2002. REDFIT: estimating red-noise spectra directly from unevenly spaced paleoclimatic time series. *Computers & Geosciences* 28, 421–426.
- Schwabe, H., 1844. *Sonnen-Beobachtungen im Jahre 1843*. *Astronomische Nachrichten* 495, 233–236.
- Solanki, S.K., Usoskin, I.G., Kromber, B., Schüssler, M., Beer, J., 2004. Unusual activity of the Sun during recent decades compared to the previous 11,000 years. *Nature* 431, 1084–1087.
- Stockhausen, H., Thouveny, N., 1999. Rock-magnetic properties of Eemian maar lake sediments from Massif Central, France: a climatic signature? *Earth and Planetary Science Letters* 173, 299–313.
- Stuiver, M., Braziunas, T.F., 1989. Atmospheric $14C$ and century-scale solar oscillations. *Nature* 338, 405–408.
- Stuiver, M., Braziunas, T.F., 1993. Sun, ocean, climate and atmospheric $^{14}CO_2$, an evaluation of causal and spectral relationships. *The Holocene* 3, 289–305.
- Stuiver, M., Grootes, P.M., Braziunas, T.F., 1995. The GISP2 $\delta^{18}O$ record of the past 16,500 years and the role of the sun, ocean and volcanoes. *Quaternary Research* 44, 341–354.
- Taricco, C., Ghil, M., Alessio, S., Vivaldo, G., 2009. Two millennia of climate variability in the Central Mediterranean. *Climate of the Past* 5, 171–181.
- Tiwari, M., Ramesh, R., 2007. Solar variability in the past and palaeoclimate data pertaining to the southwest monsoon. *Current Science* 93, 477–487.
- Usoskin, I.G., Solanki, S.K., Schüssler, M., Mursula, K., Alanko, K., 2003. A millennium scale sunspot number reconstruction: evidence for an unusually active sun since the 1940s. *Physical Review Letters* 91, 211101.
- Vasiliev, I., de Leeuw, A., Filipescu, S., Krijgsman, W., Kuiper, K., Stoica, M., Briceag, A., 2010. The age of the Sarmatian-Pannonian transition in the Transylvanian Basin (Central Paratethys). *Palaeogeography, Palaeoclimatology, Palaeoecology* 297, 54–69.
- Versteegh, G.J.M., 2005. Solar forcing of climate. 2: evidence from the past. *Space Science Reviews* 120, 243–286.
- Vos, H., Sanchez, A., Zolitschka, B., Brauer, Negendank, J.F.W., 1997. Solar activity variations recorded in varved sediments from the crater lake of Holzmaar – a maar lake in the Westeifel volcanic field, Germany. *Surveys in Geophysics* 18, 163–182.
- Wagner, G., Beer, J., Masarik, J., Muscheler, R., Kubik, P.W., Mende, W., Laj, C., Raisbeck, G.M., Yiou, F., 2001. Presence of the solar de Vries cycle (205 years) during the last ice age. *Geophysical Research Letters* 28, 303–306.
- Warrier, A.K., Shankar, R., 2009. Geochemical evidence for the use of magnetic susceptibility as a paleorainfall proxy in the tropics. *Chemical Geology* 265, 553–562.
- Weber, M.E., Tougiannidis, N., Kleineder, M., Bertram, N., Ricken, W., Rolf, C., Reinsch, T., Antiniadis, P., 2010. Lacustrine sediments document millennial-scale climate variability in northern Greece prior to the onset of the northern hemisphere glaciation. *Palaeogeography, Palaeoclimatology, Palaeoecology* 291, 360–370.
- Weedon, G., 2003. Time-Series analysis and cyclostratigraphy – examining stratigraphic records of environmental cycles. Cambridge Univ., Press, Cambridge.
- Wolf, R., 1862. *Astronomische Mitteilungen Zürich* 14.
- Xapso, M.A., Burke, E.A., 2009. Evidence of 6,000-year periodicity in reconstructed sunspot numbers. *Solar Physics* 257, 363–369.
- Yin, Z.Q., Ma, L.H., Han, Y.B., Han, Y.G., 2007. Long-term variations of solar activity. *Chinese Science Bulletin* 52, 2737–2741.
- Yousef, S.M., 2006. 80–120 yr long-term solar induced effects in the earth, past and predictions. *Physics and Chemistry of the Earth* 31, 113–122.
- Züschin, M., Hohenegger, J., 1998. Subtropical Coral-reef associated sedimentary facies characterized by mollusks (Northern Bay of Safaga, Red Sea, Egypt). *Facies* 38, 229–254.